# Chapter 2

# ACCELERATOR AUGMENTATION

## 2.1 High current injector

Sugam Kumar, R. V. Hariwal, Kedar Mal, P. S. Lakshmi, Sarvesh Kumar, Sejal Chandna, Thomas Varughese, Rajeev Ahuja, V. V. V. Satyanarayana, Parmanand Singh, Yaduvansh Mathur, S. Venkataramanan, Ashish Sharma, Chandra Pal, Ashok Kothari, P. Barua, Ruby Shanthi, Deepak K. Munda, Kundan Singh, R. K. Gurjar, Mukesh Kumar, A. Sarkar, G. O. Rodrigues, C. P. Safvan and Rajeev Mehta

The High Current Injector (HCI) project at IUAC was conceived to overcome the low-current limitations of the existing Pelletron and to enable acceleration of a broader range of ion species, including noble gases, which are otherwise inaccessible. The HCI system comprises an 18 GHz high-temperature superconducting Electron Cyclotron Resonance Ion Source (HTS-ECRIS, named PKDELIS), a multi-harmonic buncher, a 48.5 MHz Radio Frequency Quadrupole (RFQ), three 48.5 MHz spiral bunchers, and six Interdigital H-mode drift tube linac (IH-DTL) cavities operating at 97 MHz. A photograph of the HCI facility showing the installed components is shown in Fig. 2.1.

**Figure 2.1:** Photograph of the HCI facility at IUAC, showing major components including HTS-ECRIS, RFQ, spiral bunchers, and IH-DTL cavities.

The RFQ accelerates ions from 8 keV/u to 180 keV/u, while the IH-DTL cavities further boost the energy to the target value of 1.8 MeV/u. Initiated in 2005–2006, the HCI was envisioned to provide beam intensities in the range of tens of $e\mu$A and to supply a wide spectrum of ion species from across the periodic table, including noble gases and metallic ions to meet the growing demands of user experiments.

With its higher beam current capability, HCI enables investigations of nuclear reactions with extremely low cross-sections and facilitates the generation of highly charged ions suitable for injection into the superconducting linear accelerator (SC-linac). Recently, a $Ne^{7+}$ beam was successfully accelerated through all accelerating structures to its design energy of 1.8 MeV/u, thereby validating the transverse beam optics and overall system design.

### 2.1.1 ECR ion source

The HTS-ECR ion source is operational for extracting ion beams with the required charge-to-mass ratio ($A/q \leq 6$) for various beam tests as part of the commissioning of HCI. Various charge states of inert gases such as $^{20}$Ne, $^{40}$Ar, $^{84}$Kr, and $^{129}$Xe have been successfully developed from the ion source. Fig. 2.2 shows the charge state distribution spectra for Ne, Ar and Kr plasmas. Different isotopes and beams with nearby $A/q$ values have been separated using a double slit installed after the analyzer magnet.

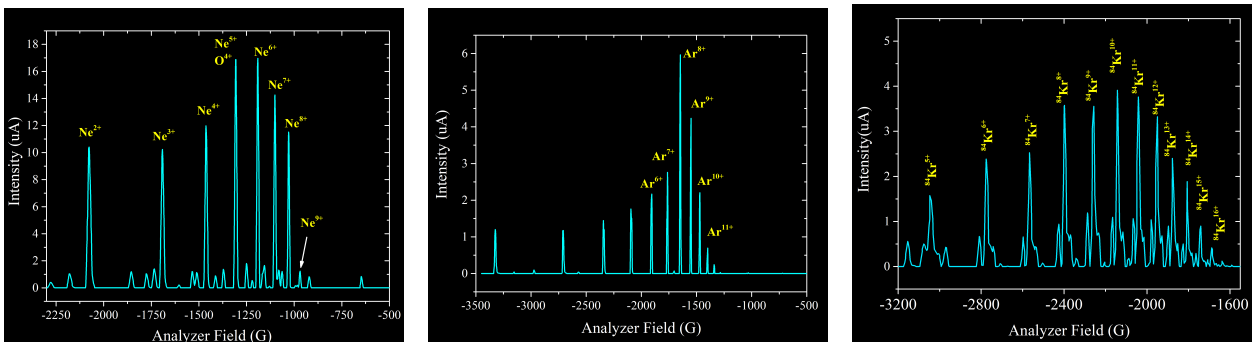


**Figure 2.2:** Charge state distribution spectra of Ne, Ar and Kr plasmas (from left to right) extracted from the HTS-ECR ion source.

The source has been operated at 18 GHz using a Klystron amplifier delivering 1.7 kW of RF power. Remarkably, the Klystron has been operated continuously for several years without major breakdowns. However, it eventually failed after approximately 24,000 hours of filament operation. As an alternative, a 250 W, 8–18 GHz TWT amplifier has been installed and coupled to the ECR ion source. A new exhaust duct was fabricated and installed to maintain the TWT temperature at around 60°C. The TWT body has been covered with Pb sheet for radiation shielding. A new server has also been added for TWT remote operation to avoid interference with the main control (PCLI) program.

An old, ruptured nylon pipe and the de-ionizer cartridge were replaced in the source cooling water line, and a turbo pump was replaced with a new one during the last academic year.

**Table 2.1:** Beam current measured at different locations along the HCI beamline.

| Location | Beam current |
|---|---|
| After analyzer magnet on HV platform | 1.4 $\mu$A |
| RFQ entrance | 700 nA |
| Exit of first achromat magnet | 150 nA |
| Exit of fourth achromat magnet | 90 nA |

Efforts have also been made to develop a Ti beam using the micro-oven method. The micro-oven system (Fig. 2.3) works up to a temperature of 1400°C. The vapour pressure of Ti at 1300°C is in the order of $10^{-5}$ mbar. Ti samples in the form of thin strips were used. A 60 V power supply was installed and tested remotely. An isolation valve was used to move the oven assembly in a vacuum inside the source chamber. However, no signature of Ti beam was observed even at the maximum power level of the TWT amplifier, likely due to insufficient vapour pressure at the highest achievable temperature. The sputtering technique will be explored as an alternative method for Ti beam development.

The first user experiment using a $^{20}Ne^{9+}$ beam with a total energy of 36 MeV (1.8 MeV/u) from the High Current Injector (HCI) was carried out on the materials science beam line in BH-II to study the electrical

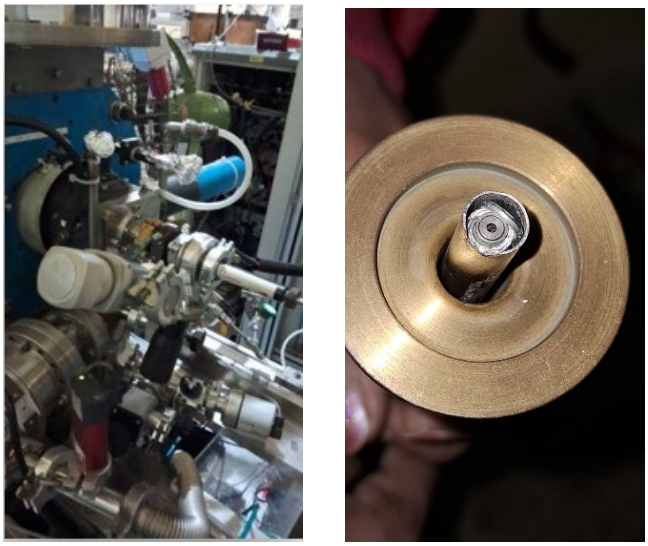

**Figure 2.3:** (Left) Micro-oven assembly installed at the injection side of the HTS-ECR ion source and (right) Close-up view of the micro-oven used for titanium beam development.

properties of porous Si. The $^{20}Ne^{9+}$ ($A/q = 2.2$) beam from the HTS-ECR ion source was accelerated to the required energy of 160 keV by the extraction potential of 17.77 kV, and no deck potential was used.

The optimized power of the TWT amplifier was found to be 185 W, and the source was operated with a single gas. To enhance the beam current, the double slit at the exit of the analyzer magnet on the HV deck was kept fully open (±15 mm). The maximum analysed beam current obtained from the ion source was 1.4 $\mu$A. The beam stability was measured to be approximately 2%. Fig. 3.25 shows the temporal stability of the ECR ion source.

The measured bunch width of the beam from the Multi-Harmonic Buncher (MHB) was 7 ns. Bunch width optimization was carried out by maximizing the analysed beam current at the exit of the first achromat. All transverse components in the MEBT section, and the RF power and phase settings of each cavity, were tuned sequentially to optimize the analysed beam current for each energy stage.

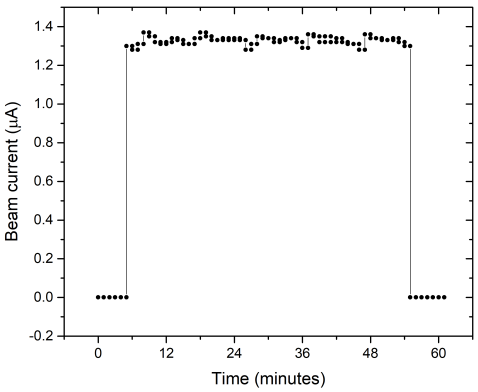


**Figure 2.4:** Stability of $Ne^{9+}$ beam measured at Faraday Cup 1.

Beam current values measured at various locations along the HCI beamline are shown in Table 2.1. The measured transmission through the Low Energy Beam Transport (LEBT) section was 50%, and through the RF cavities, it was 22%. A maximum transmission of 70% was achieved through the High Energy Beam Transport (HEBT) section. The transmission through the zero-degree linac line was 57%, where all linac cavities were used in drift mode.

Eight silicon samples were irradiated in the Materials Science-II chamber in BH-II with different fluences. The experiment was carried out in 8 beam time shifts, with an average current of approximately 5 pnA.

### 2.1.2 Multi-harmonic buncher

The Multi-Harmonic Buncher (MHB) operates at a fundamental frequency of 12.125 MHz, with second and third harmonics at 24.25 MHz and 36.375 MHz, respectively. It converts the continuous (DC) beam from the ion source into pulses of full width at half maximum (FWHM) greater than 2 ns. The bunched beam is subsequently focused at the RFQ entrance for further acceleration.

The inherent energy spread at the exit of the MHB is approximately 2%, while the energy spread at the RFQ exit is reduced to about 0.2%. However, during the most recent HCI-linac beam acceleration test, a significantly large energy spread was observed, which prevented further acceleration through the remaining linac cavities.

It is therefore necessary to reduce the inherent energy spread introduced by the MHB. Ongoing efforts aim to address this issue and achieve an energy spread below 1% and a bunch width of around 2 ns.

### 2.1.3 Radio-frequency quadrupole

The Radio-Frequency Quadrupole (RFQ) accelerates ions from 8 keV/u to 180 keV/u while providing transverse focusing. The RFQ structure is 2.5 meters long and operates at a frequency of 48.5 MHz with an inter-vane voltage of 70 kV. It is powered by a 120 kW, 48.5 MHz RF amplifier (M/s QEI Corp., USA), and has so far been operated at power levels up to 40 kW. A new coupler has recently been installed to support higher power operation, up to 80 kW. Cooling water is circulated through the structure to maintain frequency stability. The RFQ benefits from the pre-bunched beam provided by the MHB, which enhances transmission efficiency.

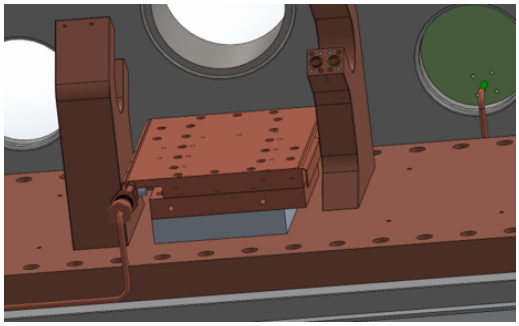

**(a)** 3D CAD view of tuning plate assembly in the RFQ cavity.

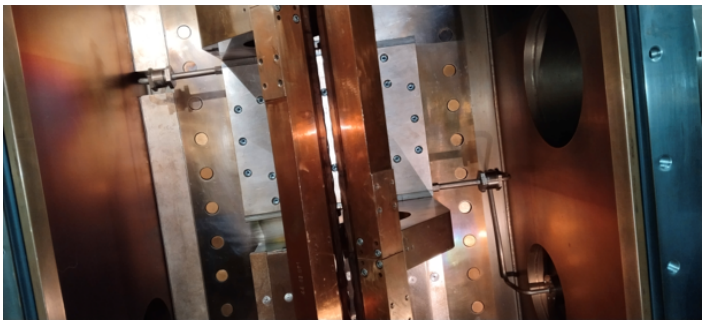

**(b)** Photograph of tuning plate installed inside the RFQ.

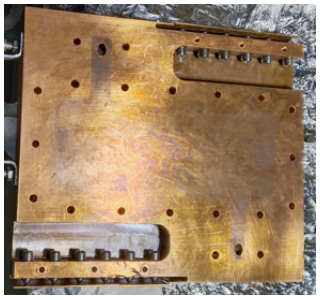

**(c)** Removed plate showing spring-plunger slots.

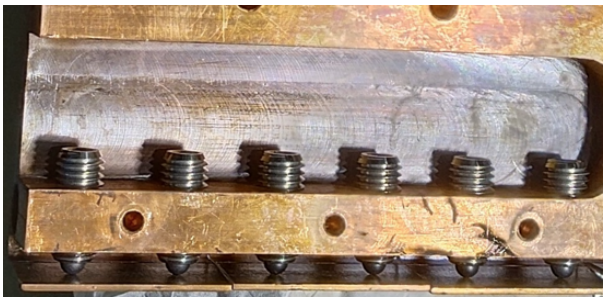

**(d)** Close-up of U-shaped contact pressed by plungers.

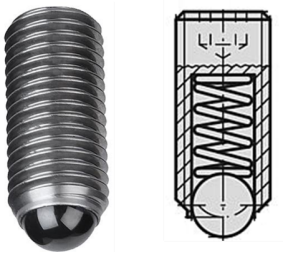

**(e)** Spring-loaded plunger.

**Figure 2.5:** Visual summary of RFQ tuning plate development and challenges. New water-cooled plates and 12 mm plungers address previous high-power failures.

One of the major challenges encountered during RFQ operation was the burning of RF contacts on the frequency tuning plates at high RF power (approximately 40 kW). The RF contacts are made by pressing a thin U-shaped copper extension of the tuning plate against the RFQ stem using spring plungers. Fig. 2.5 illustrates the tuning plate development in detail.

Initially, the RFQ was operated using tuning plates fitted with 8 mm diameter spring plungers (Fig. 2.5e). These plungers, however, suffered from frequent spring failures due to excessive localized heating, particularly at RF power levels approaching 40 kW. Additionally, these plates lacked direct water cooling and were instead cooled passively via conduction through the mounting base, which proved insufficient.

To overcome these issues, a second design iteration was tested using brazed Be-Cu finger strips in place of spring plungers. While this approach showed better electrical contact initially, it also failed at around 30 kW due to insufficient heat dissipation. These plates also relied only on indirect thermal conduction for cooling.

In the final and currently adopted solution, a new tuning plate was developed incorporating 12 mm diameter spring plungers and integrated water cooling channels throughout the RF contact region. This configuration significantly improved the thermal stability and mechanical reliability of the contacts. Fig. 2.5a shows a 3D CAD model of the redesigned tuning plate assembly. Fig. 2.5b captures the actual installed plate

in the RFQ cavity. Fig. 2.5c displays the complete plate removed from the cavity, while Fig. 2.5d focuses on the critical U-shaped contact region pressed by spring plungers. The spring-loaded plunger component itself is shown in Fig. 2.5e.

These improvements are expected to enable successful RFQ operation at higher power levels, potentially up to 90 kW, which is essential for accelerating beams with $A/q = 6$. Conditioning with the new configuration is currently ongoing.

### 2.1.4 Spiral buncher

The Spiral Buncher system consists of three spiral-type quarter-wave ($\lambda/4$) resonators operating at 48.5 MHz. These are designed for high shunt impedance and mechanical stability. The first spiral buncher, placed upstream of the first DTL cavity, bunches the beam to 1 ns (FWHM) and ensures proper longitudinal matching at the DTL entrance. This requires up to 1 kW of RF power to achieve a gap voltage of 80 kV.

To minimize longitudinal emittance growth, two additional spiral bunchers are installed in the High Energy Beam Transport (HEBT) section. These help ensure optimal beam quality throughout the transport and acceleration process.

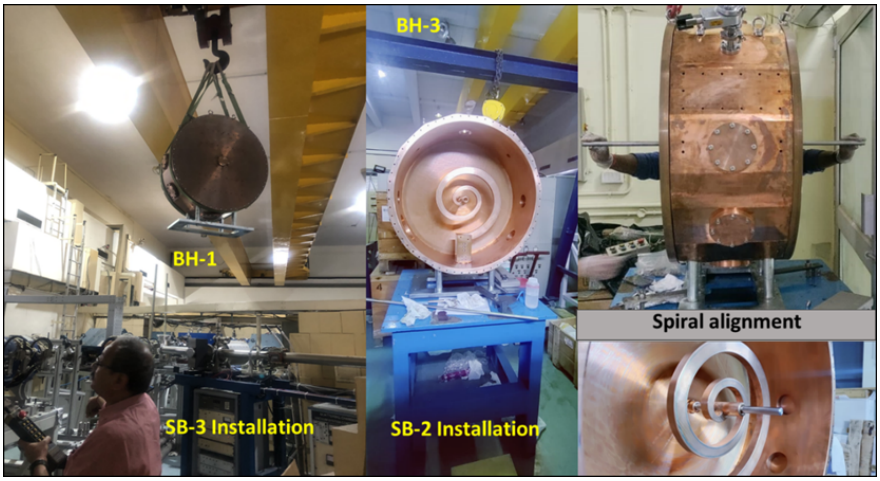


**Figure 2.6:** Pictures of installation of Spiral Bunchers 2 and 3 in BH-3 and 1 respectively.

The first spiral buncher has already been installed and tested. SB-2 and SB-3 are also installed in the HEBT line. During the last HCI–linac test, SB-3 was operated and successfully bunched the $Ne^{7+}$ beam to 1 ns, which was measured at the SBD. Conditioning of SB-2 to full power is currently in progress, and it will be tested with beam during the next beam run.

### 2.1.5 Drift tube linac

The Drift Tube linac (DTL) system has six normal-conducting Interdigital H-mode (IH-DTL) cavities that operate at 97 MHz. These cavities accelerate the ion beam from 180 keV/u to 1.8 MeV/u. To focus the beam sideways (transversely), small quadrupole triplets are placed between the DTL cavities. For focusing along the beam path (longitudinally), special bunching sections are included in the first three RF gaps of DTL-2 to DTL-5.

These DTL cavities operate in continuous wave (CW) mode and are designed to reduce the capacitive load on the accelerating electrodes, helping generate strong longitudinal electric fields for effective acceleration. The beam dynamics were optimized using the KONUS method (Kombinierte Null Grad Struktur), which improves beam stability and acceleration efficiency.

During testing, DTL-1 to DTL-4 reached their design power levels of 5 kW, 11 kW, and 18 kW. DTL-5 and DTL-6 were conditioned up to 18 kW and 20 kW, slightly below their respective design values of 24 kW and 25 kW. A saturation effect was observed in DTL-6 beyond 8 kW forward power.

Fig. 2.7 shows three key observations during DTL-6 conditioning. As the forward power exceeds 8 kW, the reflected power and x-ray radiation levels increase sharply, indicating possible surface discharge or electron emission. At the same time, the pickup voltage shows signs of saturation. This behavior suggests that the

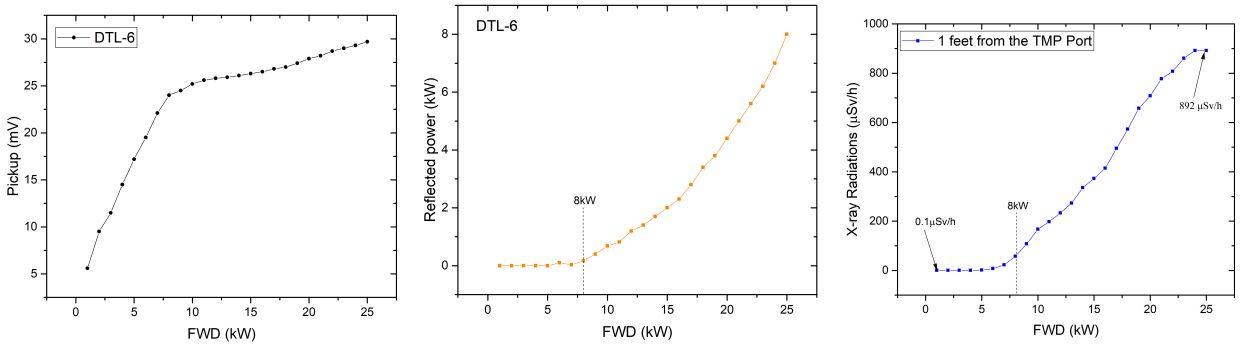


**(a)** Pickup signal vs forward power **(b)** Reflected power vs forward power **(c)** X-ray radiation vs forward power

**Figure 2.7:** Behavior of DTL-6 cavity during conditioning: reflected power and x-ray radiation increase beyond 8 kW, while pickup signal shows saturation.

cavity may not be efficiently storing additional RF energy beyond this point. The source of this saturation and radiation buildup is under investigation.

### 2.1.6 Beam acceleration tests through SC-linac

The first HCI-linac beam acceleration test involved producing a $Ne^{7+}$ beam (with $A/q = 2.86$) at an energy of 1.8 MeV/u from the HTS-ECR ion source. After optimizing the bunch length, the beam was injected into the RFQ and accelerated to 180 keV/u. It was then further bunched using Spiral Buncher-1 and injected into the six DTL cavities, accelerating it to the final design energy of 1.8 MeV/u (36 MeV). The beam currents measured after Achromat-1 and Achromat-2 were 0.5 $\mu$A and 250 nA, respectively.

To avoid damage to the Surface Barrier Detector (SBD), the beam current was reduced to 30–50 nA using a slit placed before Achromat-2. The 36 MeV energy of the $Ne^{7+}$ beam was confirmed and analysed at both SBD-1 and SBD-2. With Spiral Buncher-3 in operation, the measured bunch time width was 1.08 ns, and the energy spread was 1.3%. To inject the beam into the SC-linac, it was further bunched to 854 ps using the super buncher, and this bunch length was again confirmed at SBD-2.

The test was partially successful. The $Ne^{7+}$ beam was accelerated through the first 12 cavities of the superconducting linac, achieving a total energy gain of 77 MeV. Since the energy gain from all 24 cavities would have been 41 MeV more (totaling 118 MeV), the test had to be stopped due to the large energy spread observed in the beam, which made further acceleration infeasible.

The summary of parameters for each acceleration stage from RFQ through DTL-6 is given in Table 2.2.

**Table 2.2:** Cavity parameters and performance from RFQ through DTL-6.

| Cavity Parameters | RFQ | DTL1 | DTL2 | DTL3 | DTL4 | DTL5 | DTL6 |
|---|---|---|---|---|---|---|---|
| Frequency (MHz) | 48.5 | 97 | 97 | 97 | 97 | 97 | 97 |
| Cavity Length (m) | 2.5 | 0.39 | 0.69 | 0.90 | 0.94 | 0.92 | 0.82 |
| No. of RF Gaps | 42 | 11 | 13 | 13 | 13 | 11 | 9 |
| Designed E. Gain (MeV/u) | 0.18 | 0.32 | 0.55 | 0.85 | 1.15 | 1.46 | 1.8 |
| RF Power for $A/q = 6$ (kW) | 80 | 5 | 11 | 18 | 18 | 24 | 25 |
| RF Power for $A/q = 2.86$ (kW) | 17 | 1.1 | 2.4 | 3.9 | 3.9 | 5.3 | 5.5 |
| Energy Gain (for $Ne^{7+}$) (MeV) | 3.6 | 6.4 | 11 | 17 | 23 | 29.2 | 36 |

### 2.1.7 Beam experiment with HCI

The successful commissioning of the High Current Injector (HCI) was marked by a landmark experiment conducted by Prof. Nageswara Rao S. V. S. from the Centre for Advanced Studies in Electronics Science and Technology (CASEST), University of Hyderabad, at IUAC. Prof. Rao, a distinguished researcher in the field of materials science and ion–matter interactions, led the first-ever experiment using the $Ne^{9+}$ beam produced from HCI.

In this experiment, a $Ne^{9+}$ beam with an energy of 36 MeV and a beam current of 5 pnA was bombarded onto porous silicon samples at different fluence levels ranging from $10^{14}$ to $10^{15}$ ions/cm$^2$. The main objective was to investigate the ion-induced tracks and to analyze changes in the material's properties using computational *in-silico* techniques. The morphology, size, and density of ion tracks were found to vary with fluence, offering valuable insight into the structural modifications induced by energetic ion irradiation. Further *in-silico* modeling is expected to validate the correlation between fluence and the evolution of track patterns and material stability.

This important experiment not only confirmed that the HCI is fully operational, but also showed that it can deliver high-charge-state and high-current beams. These beams are well suited for advanced experiments. With the successful commissioning of the HCI, new opportunities are now available for interdisciplinary research in materials science, nuclear physics, astro-nuclear physics, and atomic and molecular physics.

This achievement establishes IUAC as a key national center for accelerator-based research and reinforces the strategic value of HCI in supporting frontier investigations in ion–matter interactions.

## 2.2 Free electron laser based THz facility

B. K. Sahu[1], P. Patra[1], J. Karmakar[1], B. Karmakar[1], M. Aggarwal[1], A. Sharma[1], A. Kothari[1], T. Vurughese[1], G. K. Chaudhari[1], P. Barua[1], Chandrapal[1], R. Kumar[1], S. K. Suman[1], P. K. Verma[1], S. Venkataramanan[1], P. Singh[1], Abhishek Kumar[1], R. N. Dutt[1], V. V. V. Satyanarayana[1], K. Singh[1], R. Shanti[1], D. K. Munda[1], Y. Mathur[1], P. K. Mukhopadhyay[4], T. Rao[2], A. Aryshev[3], S. Ghosh[1], R. K. Bhandari[1] and A. C. Pandey[1]

[1] *Inter University Accelerator Centre, Aruna Asaf Ali Marg, New Delhi, India*
[2] *Brookhaven National Laboratory, USA*
[3] *High Energy Accelerator Research Organization, KEK, Tsukuba, Japan*
[4] *Raja Ramanna Centre for Advanced Technology, Indore, M.P., India*

A compact, pre-bunched Free Electron Laser based THz facility known as Delhi Light Source (DLS) is at its final phase of commissioning at IUAC. As reported in previous years electron beam up to 5 MeV energy is regularly produced for conducting experiments in Material Science, Biology and Atomic physics as per user requirements using solid state NdYAG Laser. This year the fiber-based laser system developed in collaboration with KEK Japan is installed at IUAC for the production of quality electron beam required for production of THz. The femtosecond electron beam from the electron gun is produced using the newly installed laser system as the reference master, and the produced electron beam is being transported into the compact undulator for the production of coherent THz radiation. The THz extraction chamber is made equipped with a Ti-foil to reflect THz radiation at 45-degree angle which is installed post undulator section. Detection of THz radiation coming from both Coherent Transition Radiation and undulator radiation is being explored using a pyroelectric detector. Alongside the deposition of new photocathodes are also undertaken to increase the charge produced from the source. The RF Conditioning of the photocathode gun continued in order to increase the electric field inside the RF Gun and to reduce the dark current. This year, the beam line from dipole magnet-1 has been extended up to the beam dump post dipole magnet-2. Now the complete beam line is equipped with both the dipole magnets of the 60 degree achromatic bends and two electron experimental chambers are installed, one pre undulator and another after the second dipole.

### 2.2.1 Status of various subsystems of DLS

The progress of the various activities related to the setting up of the compact FEL is listed in the following subsections:

#### 2.2.1.1 Commissioning status of the electron beam line

During the last academic year, in addition to the first dipole magnet used for the energy measurement of the electron beam, the second dipole magnet along with the magnetic quadrupole triplet and steering magnets was installed to complete the achromatic bend section of the electron beam. In this academic year, the 60° bending section of the second dipole magnet is aligned with precision with the diagnostic chamber, beam position monitors along with quadrupole doublets, and steering magnet for the delivery of the electron beam up to the experimental chambers for electron beam related experiments. All the magnets, Beam

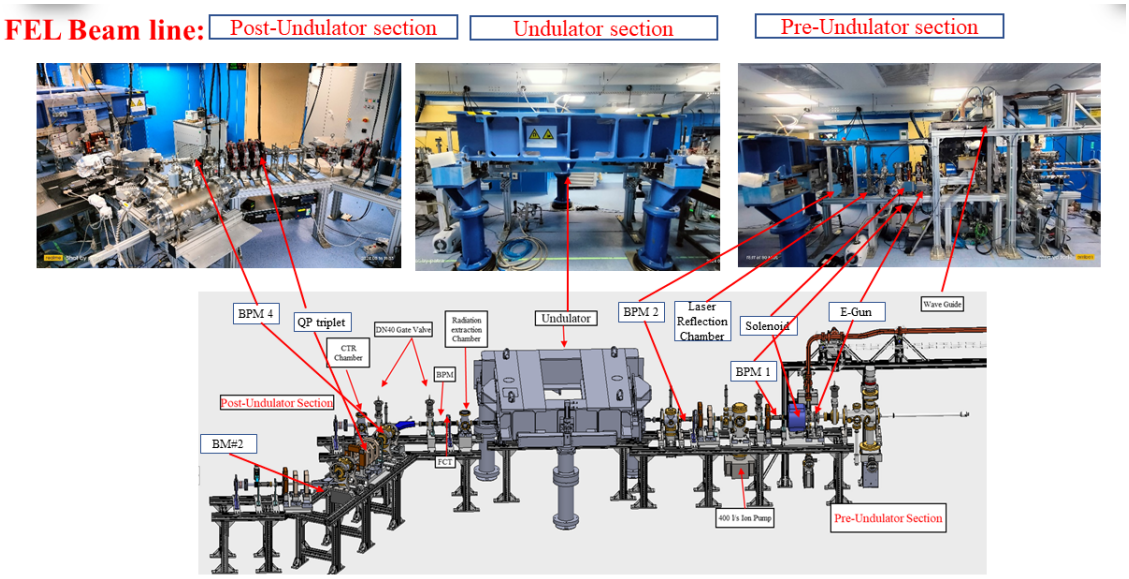


**Figure 2.8:** : The complete beam line for post undulator section along with the second dipole magnet and the quadrupole triplet

**Table 2.3:** Experiments using electron beam facility of FEL.

| User Affiliation | Experiments | Energy of the electron beam | Total beam time (hours) |
|---|---|---|---|
| CCU Meerut | Low energy electron beam affecting physiological and biochemical attributes of garden Pea plant with ZnO particle. | 5 MeV | 24 |
| IIT Hyderabad | Sample type CVD grown 2D MoS2 on SiO2/Si (Thin film), sample size 5x5mm | 1 MeV | 48 |
| IIT Delhi | Irradiation of CVD grown thin film of 2D material Res2 at different fluences to study optical, morphological and electrical spectra | 1-5 MeV | 27 |

Position monitors, Beam viewers, ICTs, Ion pumps etc. are installed with respective power supplies control system and transmission of the electron beam through the bend section is tested. The optimization of beam transmission is continuing. The view of the completed beam line post-undulator section along with design drawings of the entire beam line is shown in Fig. 2.8. During the last academic year, a nanosecond UV laser having wavelength range (266 nm) was made to incident on the cathode to produce electrons from copper photocathode, and the same is being used by various users for conducting experiments with the available electron beam. In this academic year, three experiments were conducted using the FEL electron beam facility as listed in Table 2.3.

### 2.2.2 Installation and testing of the fibre laser system

The laser system is one of the most crucial subsystem of the DLS facility for the production of THz. Last academic year the development and testing of fibre laser developed by FEL laser group in collaboration with KEK and with experts helps from RRCAT at KEK was reported. This year the system has been shipped to IUAC and the whole system was reassembled and commissioned at IUAC. The Laser system is capable producing multi micro bunch structure which will be useful for generating high intensity THz radiation from FEL. The laser system has been used as master in up conversion configuration to power the electron gun and to produce multi micro bunch femtosecond electron beam bunches. The development of the laser system is successfully completed and the multi micro bunch structure electron beam is produced on regular basis by using the Fiber Laser system at IUAC. The installed fiber laser system inside IUAC laser room along with the measured parameters are shown in Fig. 2.9.

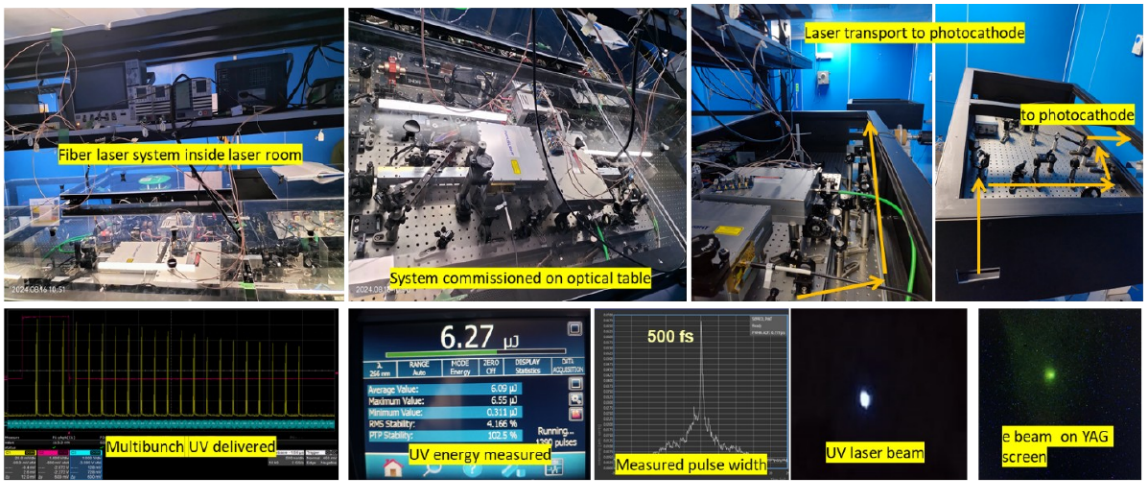


| | |
|---|---|
| **Pulse width (FWHM)** | **~500fs** |
| **Burst Energy (IR)** | **2-3 mJ (1030nm)** |
| **Burst Energy (Green)** | **~200µJ (515nm)** |
| **Burst energy (UV) Max** | **~10 µJ (258nm)** |
| **Capable of splitting single pulse into 4 micropulses** | |

**Figure 2.9:** The installed fiber laser system inside IUAC laser room along with the measured parameters

### 2.2.3 Development of laser and RF synchronization by up-conversion scheme

After the successful installation of pulsed fiber laser system, synchronization of the 130 MHz laser oscillator pulses with the 2860 MHz RF signal with $< 10$ ps jitter was necessary to produce stable electron beam. There are two approaches to achieve the synchronization viz. either by making 2860 MHz RF signal as master or by making 130 MHz laser signal as master. The later approach where 130 MHz was up-converted to 2860 MHz and used for powering the RF gun was tried and successfully implemented to achieve the synchronization. In this up-conversion scheme mostly commercially available RF components like frequency mixers, multipliers, attenuators, amplifiers, band pass filters were used. Apart from this one voltage-controlled phase shifter has been used to control the relative phase between the RF signal and laser pulses, a variable attenuator is used for controlling the signal amplitude and a very narrow band ($\pm$25 MHz) filter at 2860 MHz has been used at the final stage to get a spectrally pure 2860 MHz signal. A relative phase jitter of $\sim$ 5 ps has been measured between the synchronized laser oscillator frequency and RF Photocathode gun drive frequency signals. The up-conversion unit is being regularly used for generation of stable electron beam whereas the synchronization of Laser frequency with master cavity frequency is being explored for stability requirements at higher RF power. The block diagram of the up-conversion scheme along with the actual unit is shown in the Fig. 2.10.

### 2.2.4 Production of electron beam using fibre laser system and detection of 2 and 4 electron micro-bunches

Initially the electron beam was produced by a single laser pulse from the Fibre laser system. After the generation of stable electron beam, the first detection of the laser pulse splitting into 2 and 4 micro pulses was done through the observation of the subsequently generated 2 and 4 electron micro-bunches observed in the YAG screen at 1.4m downstream of the RF gun. The schematic of the laser pulse splitter (laser buncher) is shown in Fig. 2.11. In order to detect the splitting, the generated electron beam was observed in the YAG screen and the solenoid was operated with beam in off-axis mode so as to induce steering in the beam. By varying the phase of laser oscillator, RF energy modulation was induced into the micro-bunches as a result they could be separated and seen in the YAG screen as shown in the Fig. 2.11. For the 4 pulse splitting

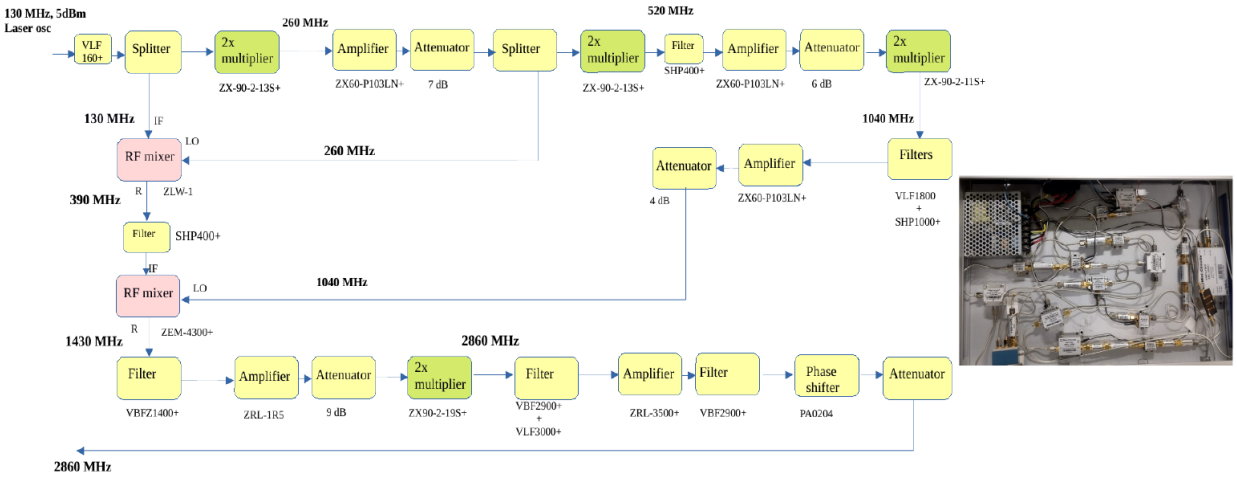


**Figure 2.10:** (Left) Schematic of up-conversion module and (right) the actual module.

the energy modulation was large enough for the fixed solenoid field to keep the fourth bunch focused. The splitting was confirmed by blocking the mirrors in the buncher one by one.

### 2.2.5 Development of a compact Faraday cup for detection and measurement of MHz multi micro bunch electron beam produced using fiber laser system

As discussed in the previous section, the fiber laser system of the DLS could provide complicated multi-micro pulse laser structures that are capable of producing similar kind of electron bunch structure with sub pico-second temporal width. Individual pulses are not distinguishable using commercial available beam position monitors (BPM) or integrated current transformers (ICT). The development of a compact faraday cup is carried out in-house using OHF copper material. The developed faraday cup has been used not only to distinguish the multi micro pulse structure but also gave quite correct estimation of the photocurrent generated by the laser pulses. Currently one Faraday Cup has been installed just after the laser insertion chamber and two more are kept ready for installation in subsequent diagnostic chambers in future to estimate the electron beam transport along the beam line. The same is being calibrated using the commercial ICT which is already installed. The installed faraday cup and the detected electron beam structure is shown in Fig. 2.12

### 2.2.6 Production and detection scheme of THz using DLS facility

As discussed in previous sections, Currently the electron beam having energy up to 6 MeV has been produced with sub pico Coulomb (pC) of charge from the copper photocathode inserted inside the RF Photocathode Gun. The same beam is being planned to be used for THz generation by passing it through the undulator field as well as by passing it through a Aluminum/Titanium reflecting surface for production of Coherent THz radiation. The plan to detect the THz radiation produced by the beam has started along with the efforts to increase the THz intensity. The current detection measurements of narrowband coherent undulator radiation (CUR) and the broadband coherent transition radiation (CTR) have been finalized using pyroelectric and SBD detectors. The testing of the detectors (including the calibration of transportation components) has been performed with known THz source prior to its characterization at the DLS facility. The responsivity of detectors and their polarization sensitivity in addition to the transmission curves of viewport and lens have been obtained in the desired frequency range. Based on these calibrations, the finalization of the detection scheme is employed with the expected THz intensity.

The DLS facility has been designed to produce the THz radiation using undulator source. Simulations have been performed previously using designed 10s of pC of charge from the RF photocathode. Currently efforts to increase the electron beam charge using semiconductor photocathode are in progress, as the charge produced using Cu photocathode is quite less ( 100 fC). Along with the radiation from the undulator, parallel schemes have been implemented for the detection of CTR. CTR is produced when the electron beam is incident on the vacuum-dielectric surface, resulting in emission of electromagnetic radiation due to rapid

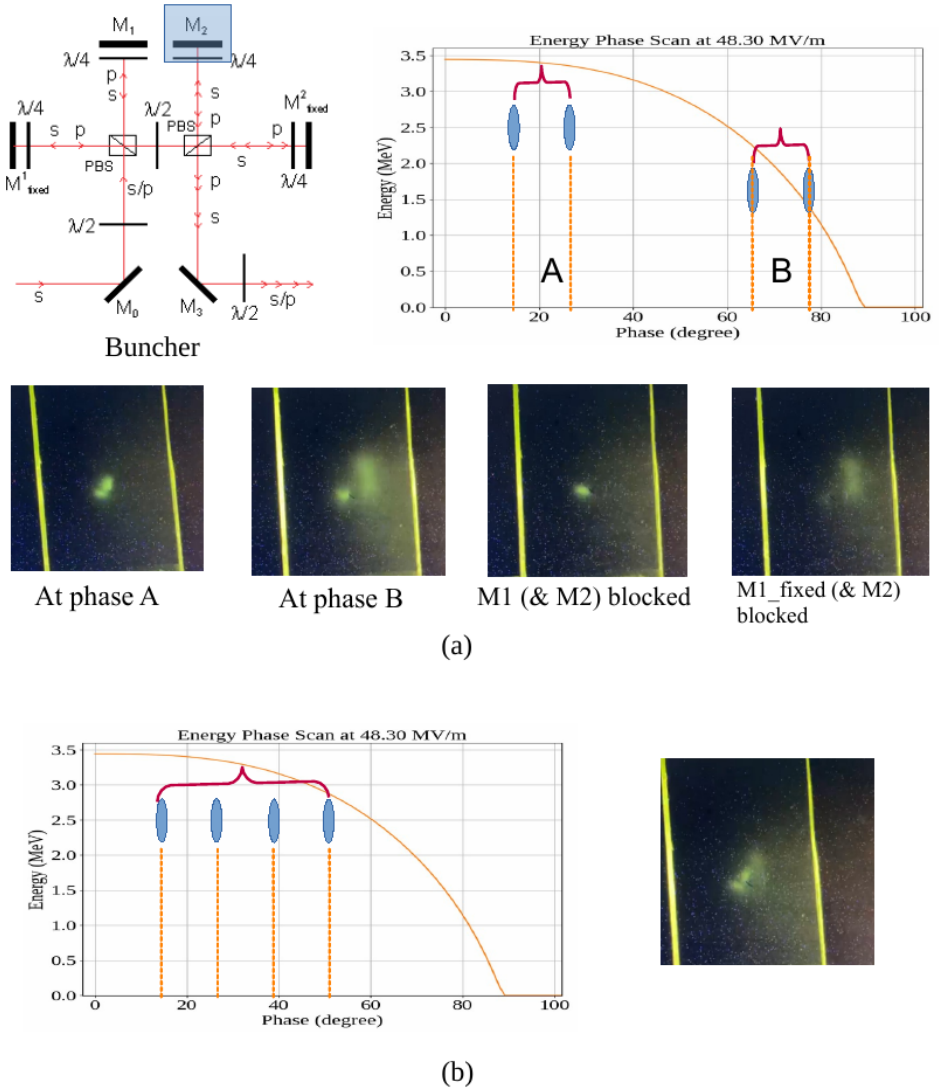


**Figure 2.11:** Laser buncher and energy phase scan diagram for (a) detection of two pulse splitting and (b) four pulse splitting by making use of the energy phase slope and varying the phase.

rearrangement of the electric field during the transition through the two media. Unlike narrowband tuneable coherent undulator radiation (CUR), CTR is broadband, emitting radiation of all frequencies with a higher cut off frequency. The end frequency depends on the electron bunch length, which comes out to be around few tens of THz for ps bunch widths. To establish the detection scheme, it has been decided to measure the radiation using both CTR and CUR using available detectors. The detection schemes for both CUR and CTR are shown in Fig. 2.13

In order to test the performance and sensitivity of the available detectors, they are characterized using standard source. The complete setup of detection includes a radiation source, viewport, lens, detector (pyroelectric and SBD) and an RF pre-amplifier both for CTR as well as CUR. The SBD detector received from KEK has also been tested with the same source. The detector is found to have flat response in its frequency range 90-140 GHz with responsivity of around 200 V/W at 100 GHz (input power is 100 µW at 100 GHz). The order of responsivity is matching with the datasheet (400 V/W), whereas exact calculation requires more intense measurements with proper focusing and calibration of the source taking into account the ambience etc. The complete characterization of the detection setup has been performed. The trials for detecting the initial signature of radiation are ongoing along with parallel efforts to increase the THz intensity for better detection efficiency.

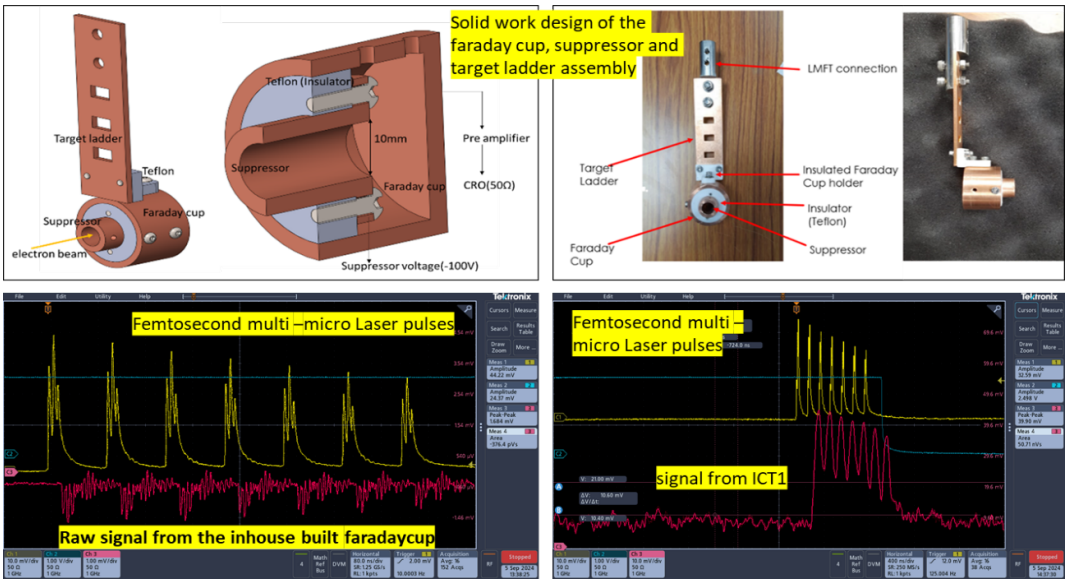


**Figure 2.12:** Installed faraday cup assembly along with the detected pulse structure in comparison with commercial ICT.

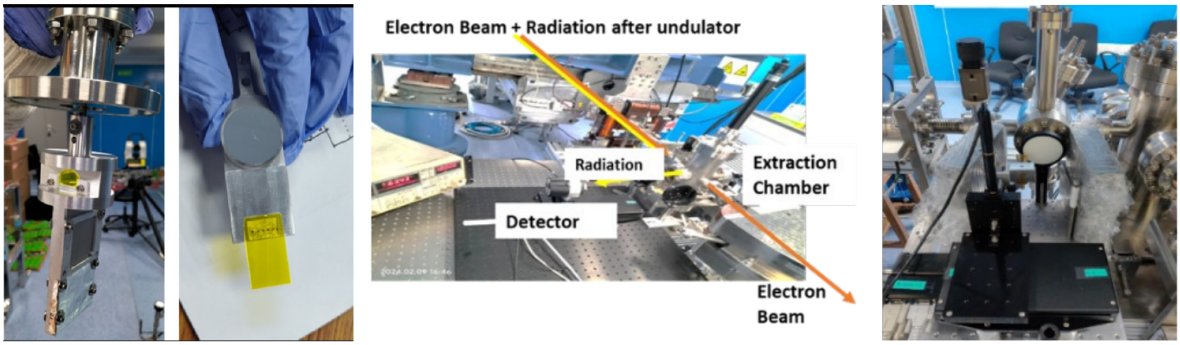


**Figure 2.13:** (a) CUR reftlector, (b) Al mirror for CTR generation, (c) CUR detection set up and (d) CTR detection set up.

### 2.2.7 Status of the photocathode deposition system at IUAC

At present, the production of electron beam is continued by injecting the laser beam on the Cu photocathode. In order to improve the charge of the electron beam so as to generate intense THz, semiconductor photocathode ($Cs_2Te$) deposition system is being installed. In the last academic year source assembly installation was completed and temperature calibration of cathode substrate was done along with the positioning of the Quartz Crystal Monitor (QCM) with respect to the substrate. This academic year, a UV LED system was installed just outside the deposition chamber to measure the quantum efficiency of the photo cathode during deposition. After installation of photocathode deposition system along with other accessories like vacuum elements, magnetic manipulators, source chambers etc., the whole system was made leak tight with an achieved leak rate of $5^{-12}$ mbar l/s and different pumping and baking processes were followed to achieve ultra-high vacuum. Source assembly installation was also completed. Different calibration processes like temperature calibration of the cathode substrate, Quartz Crystal Monitor (QCM) calibration for thickness measurement of the cathode film were also completed. The first deposition of $Cs_2Te$ photocathode on Cu substrate has been demonstrated and a QE of $2 \times 10^{-3}$ has been achieved. Now efforts are being put to optimize the deposition process to increase the QE of the semiconductor photocathode on Cu substrate. Once we get a QE of $10^{-2}$ to $10^{-1}$, it is planned to be inserted into the RF gun for actual operation.